

## 1 Test Beam Studies Of Silicon Timing for Use in Calorimetry.

2 A. Apresyan<sup>a</sup>, G. Bolla<sup>b</sup>, A. Bornheim<sup>a</sup>, H. Kim<sup>c</sup>, S. Los<sup>\*,b</sup>, C. Pena<sup>a</sup>, E. Ramberg<sup>b</sup>,  
3 A. Ronzhin<sup>b</sup>, M. Spiropulu<sup>a</sup>, S. Xie<sup>a</sup>4 <sup>a</sup>*California Institute of Technology, Pasadena, CA, USA*  
5 <sup>b</sup>*Fermi National Accelerator Laboratory, Batavia, IL, USA*  
6 <sup>c</sup>*University of Chicago, Chicago, IL, USA*7 **Abstract**

8 The high luminosity upgrade of the Large Hadron Collider (HL-LHC) at CERN is ex-  
9 pected to provide instantaneous luminosities of  $5 \times 10^{34} \text{ cm}^{-2} \text{ s}^{-1}$ . The high luminosities  
10 expected at the HL-LHC will be accompanied by a factor of 5 to 10 more pileup compared  
11 with LHC conditions in 2015, further increasing the challenge for particle identification  
12 and event reconstruction. Precision timing allows to extend calorimetric measurements  
13 into such a high density environment by subtracting the energy deposits from pileup  
14 interactions. Calorimeters employing silicon as the active component have recently be-  
15 come a viable choice for the HL-LHC and future collider experiments which face very  
16 high radiation environments. In this article, we present studies of basic calorimetric and  
17 precision timing measurements using a prototype composed of tungsten absorber and sil-  
18 icon sensor as the active medium. We show that for the bulk of electromagnetic showers  
19 induced by electrons in the range of 20 GeV to 30 GeV, we can achieve time resolutions  
20 better than 25 ps per single pad sensor.

21 *Key words:*

22 Silicon, Timing, Calorimeter

23 **1. Introduction**

24 Future colliders, including the high luminosity upgrade of the Large Hadron Col-  
25 lider (HL-LHC) at CERN, will operate with an order of magnitude higher instantaneous  
26 luminosity compared to what has been achieved at the LHC so far. With the increased in-  
27 stantaneous luminosity the rate of simultaneous interactions per bunch crossing (pileup)  
28 is projected to reach an average of 140 to 200. The large amount of pileup increases the  
29 likelihood of confusion in the reconstruction of particles from the hard scatter interaction  
30 with those produced in different pileup interactions. The ability to discriminate between  
31 jets produced in the events of interests, especially those associated with the vector bo-  
32 son fusion processes, and jets produced by pileup interactions will be degraded. The

---

\*Corresponding author  
Email address: los@fnal.gov (S. Los)

33 missing transverse energy resolution will deteriorate, and several other physics objects  
34 performance metrics will suffer.

35 One way to mitigate the pileup confusion effects, complementary to precision tracking  
36 methods, is to perform a time of arrival measurement associated with a particular layer  
37 of the calorimeter, allowing for a time assignment for charged particles and photons.  
38 Such a measurement with a precision of about 20-30 ps, when unambiguously associated  
39 to the corresponding energy measurement, will reduce the effective amount of pileup by  
40 a factor of 10, given that the spread in collision time of the pileup interactions at HL-  
41 LHC is foreseen to be approximately 200 ps. The association of the time measurement  
42 with the energy measurement is crucial, and leads to a prototype design that calls for  
43 time and energy measurements to be performed in the same detector element. Since  
44 both the energy and time measurement are performed in the same detector element<sup>1</sup>,  
45 once an energy deposit is identified as originating from a pileup interaction, it can be  
46 unambiguously removed from event reconstruction.

47 Several alternative options to combine high resolution energy and timing measure-  
48 ments for calorimetry have been reported in Refs. [1–5]. In this article, we describe the  
49 continuation of this program of study using a calorimeter prototype employing a 300  $\mu\text{m}$   
50 thick silicon pad sensor of  $6 \times 6 \text{ mm}^2$  size as the active element. Silicon-based calorimeters  
51 have recently become a viable choice for future colliders due to the radiation hardness of  
52 silicon, and the ability to construct highly granular detectors [6]. An important example  
53 is the forward calorimeter proposed for the CMS Phase 2 Upgrade [7]. We study the  
54 timing properties of silicon-based calorimetry using a prototype composed of tungsten  
55 absorber and a silicon sensor produced by Hamamatsu [8]. A similar test was previously  
56 conducted at the CERN North Area, with a lead absorber followed by silicon sensors of  
57 120-320  $\mu\text{m}$  thickness [9].

58 The paper is organized as follows. General silicon timing properties and bench test  
59 results are described in Section 2. The test beam setup and experimental apparatus  
60 are presented in Section 3. The results of the test beam measurements are presented in  
61 Section 4. Sections 5 and 6 are devoted to discussion and conclusion, respectively.

## 62 2. General Properties of Silicon Timing and Bench Test Studies

63 For our measurements, we used a silicon sensor produced by Hamamatsu [8]. The  
64 thickness of the silicon was measured to be 325  $\mu\text{m}$ . The transverse size of the sensor  
65 is  $6 \times 6 \text{ mm}^2$ . The negative bias voltage was applied to the p-side of the silicon. The  
66 capacitance of the silicon diode is measured as a function of the bias voltage and shown  
67 in Figure 1. We observe that the silicon is fully depleted above about 120 V. Timing  
68 measurements are expected to improve with larger bias voltage as the carrier velocity  
69 increases.

70 The electric diagram of the silicon diode connections is presented in Figure 2. At-  
71 tention was paid to provide good filtering for bias voltage, to reduce ground loop effects,  
72 and to minimize inductive loop for the signal readout. The timing characteristics of the  
73 signal pulses are dominated primarily by properties of the silicon sensor rather than the  
74 details of the circuit.

---

<sup>1</sup>If there are no overlapping energy deposits in the same detector element from multiple particles.

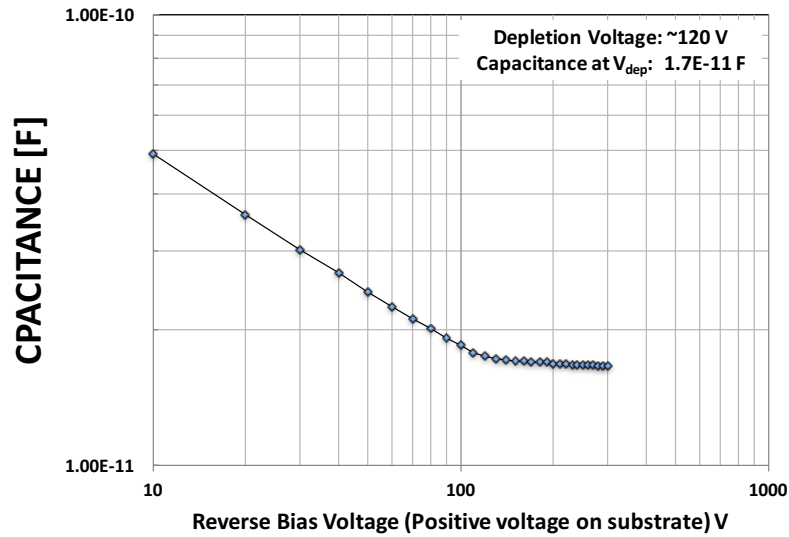


Figure 1: The measured capacitance as a function of the applied bias voltage.

75 The silicon diode was placed inside a light-tight box of thickness 1.5 cm, which also  
 76 provides electromagnetic shielding. The box is made of 0.2 mm steel. The bias voltage  
 77 was supplied to the circuitry by a cable with a balun filter, terminated with an SHV  
 78 connector. The silicon diode output signal is read out through an SMA connector elec-  
 79 trically grounded to the box. The dark current was measured at several values of the  
 80 bias voltage. The maximum value of the dark current was less than 1.0 nA at  $-500$  V,  
 81 which is the largest bias voltage used in the measurements reported in this paper. The  
 82 silicon box and bench test setup are presented in Figure 2.

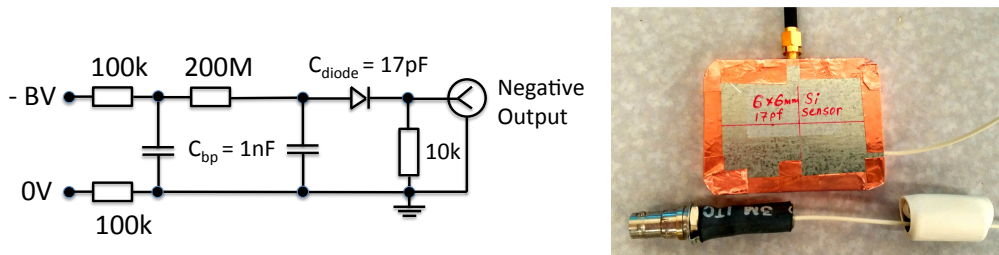


Figure 2: The electric diagram for the silicon diode connections (left). External view of the box with silicon diode, and the bias voltage connection is shown below it (right).

83 The signals from the silicon sensor were amplified by two fast, high-bandwidth pre-  
 84 amplifiers connected in series. The first amplifier is an ORTEC VT120C pre-amplifier,  
 85 and the second amplifier is a Hamamatsu C5594 amplifier. Using a pulse-generator, we  
 86 measured the combined gain of the two amplifiers in series as a function of the input  
 87 signal amplitude and found some degree of non-linearity for typical signals produced by

88 the silicon sensor under study, and we corrected for them.

### 89 3. Test-beam Setup and Experimental Apparatus

90 We performed the test-beam measurements at the Fermilab Test-beam Facility (FTBF)  
91 which provided a proton beam from the Fermilab Main Injector accelerator at 120 GeV,  
92 and secondary beams composed of electrons, pions, and muons of energies ranging from  
93 4 GeV to 32 GeV. A simple schematic diagram of the experimental setup is shown in  
94 Figure 3. A small plastic scintillator of transverse dimensions  $1.8\text{ mm} \times 2\text{ mm}$  is used  
95 as a trigger counter to initiate the read out of the data acquisition (DAQ) system and  
96 to select incident beam particles from a small geometric area, allowing us to center the  
97 beam particles on the silicon sensor. Next, we place a stack of tungsten absorbers of  
98 various thicknesses for measurements of the longitudinal profile of the electromagnetic  
99 shower. The silicon pad sensor is located within a metal box covered by copper foil,  
100 and is placed immediately downstream of the absorber plates. Finally, a Photech 240  
101 micro-channel plate photomultiplier detector [1–4] is placed furthest downstream, and  
102 serves to provide a very precise reference timestamp. Its precision was previously mea-  
103 sured to be less than 10 ps [3]. A photograph showing the various detector components  
104 is presented in Figure 4. A differential Cherenkov counter is located further upstream of  
105 our experimental setup and provides additional particle identification capability. More  
106 details of the experimental setup are described in our previous studies using the same  
107 experimental facility in references [1–4].

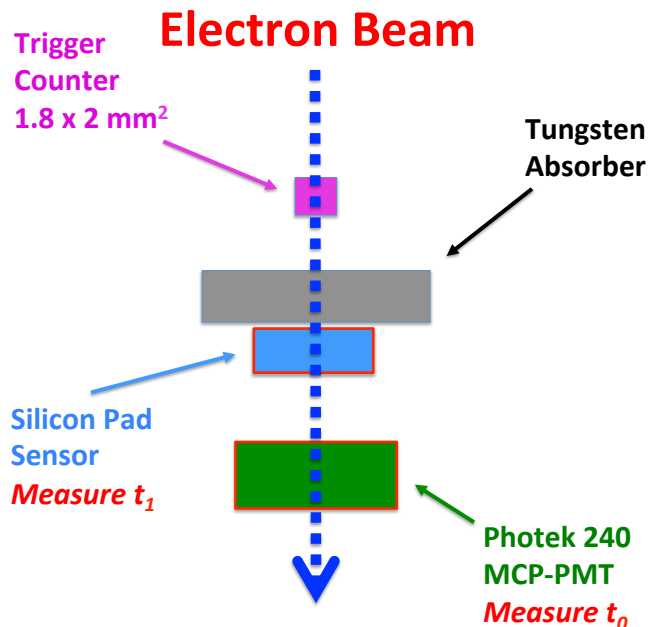


Figure 3: A schematic diagram of the test-beam setup is shown. The  $t_0$  and  $t_1$  are defined in Section 4.

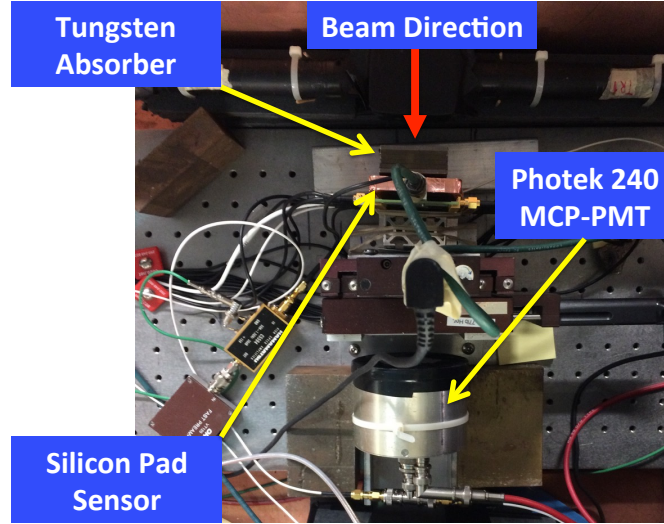


Figure 4: Test beam setup.

108 The DAQ system is based on a CAEN V1742 digitizer board [10], which provides  
 109 digitized waveforms sampled at 5 GS/s. The metal box containing the silicon sensor was  
 110 located on a motorized X-Y moving stage allowing us to change the location of the sensor  
 111 in the plane transverse to the beam at an accuracy better than 0.1 mm. A nominal bias  
 112 voltage of 500 V was applied to deplete the silicon sensor in most of the studies shown  
 113 below, unless noted otherwise.

#### 114 4. Test Beam Measurements and Results

115 Measurements were performed in 2015, using the primary 120 GeV proton beam, and  
 116 secondary beams provided for the FTBF. Secondary beams with energies ranging from  
 117  $4 \text{ GeV}/c^2$  to  $32 \text{ GeV}/c^2$  were used. Electron purity for those beams ranges between  
 118 70% at the lowest energy to about 10% at the highest energy. Stacks of tungsten plates  
 119 with varying thicknesses were placed immediately upstream of the silicon device in order  
 120 to measure the response along the longitudinal direction of the electromagnetic shower.  
 121 The radiation length of tungsten is 3.5 mm, and the Moliere radius is 9.3 mm. The  
 122 tungsten plate size is sufficient to fully contain the shower in the transverse dimension.  
 123 Signals from the silicon sensor and the Photek MCP-PMT are read out and digitized  
 124 by the CAEN V1742 digitizer, and example signal waveforms are shown in Fig. 5. The  
 125 signal pulse in the silicon sensor has a rise time of about 1.5 ns, and a full pulse width of  
 126 around 7 ns. This rise time is consistent with a time constant of a silicon sensor coupled  
 127 to a 50 Ohm amplifier.

128 The CAEN digitizer is voltage and time calibrated using the procedure described in  
 129 Ref. [11]. The total collected charge for each signal pulse is computed by integrating a  
 130 10 ns window around the peak of the pulse. The time for the reference Photek MCP-  
 131 PMT detector is obtained by fitting the peak region of the pulse to a Gaussian function  
 132 and the mean parameter of the Gaussian is assigned as the timestamp  $t_0$ . The time for

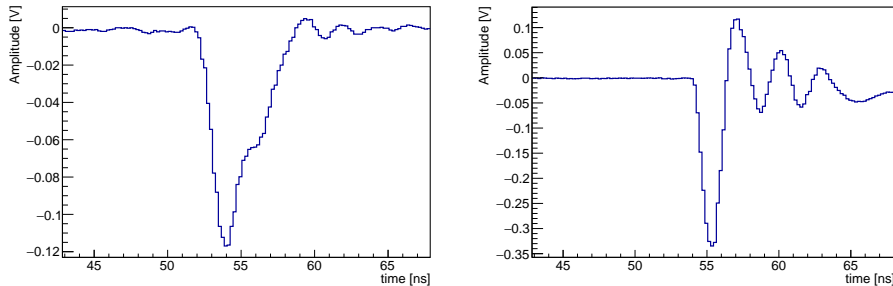


Figure 5: Examples of the signal pulse waveform for the silicon sensor (left) and the Photek MCP-PMT (right) digitized by CAEN V1742 digitizer board. The bias voltage applied to the silicon pad sensor is 500 V.

133 signals from the silicon sensor is obtained by performing a linear fit to the rising edge  
 134 of the pulse and the time at which the pulse reaches 30% of the maximum amplitude is  
 135 assigned as its timestamp  $t_1$ . We measured the electronic time resolution of the CAEN  
 136 V1742 digitizer as  $\sim 4$  ps and neglected its impact on the timing measurements described  
 137 below.

138 Electrons were identified by requiring that the signal amplitude of the gas Cherenkov  
 139 counter provided by the FTBF and the Photek detector located further downstream of  
 140 the silicon sensor exceed certain thresholds because electromagnetic showers induced by  
 141 electrons produce significantly larger signals, while pions produce much smaller signals.  
 142 After imposing the electron identification requirements the electron purity is between  
 143 80% and 90% for all beam conditions. The purity was determined by comparing the  
 144 calorimetric measurements with those from the Cherenkov detector.

145 We begin by establishing the signal characteristics of a minimum-ionizing particle  
 146 (MIP) using beams of 120 GeV protons and 8 GeV electrons with no absorbers upstream  
 147 of the silicon pad sensor. To separate MIP signals from noise, we first collect data  
 148 events with no beam and random trigger. The charge distribution for these noise runs is  
 149 presented in Fig. 6. As expected, the charge distribution is centered at 0, and the RMS  
 150 is about 2 fC.

151 In Figure 7, we show silicon sensor response to 120 GeV protons and 8 GeV electrons  
 152 without any absorber. We observe very similar response for these two cases, and  
 153 measure peak integrated charge of 4.5 fC and 5.0 fC respectively. The measured signal  
 154 is corrected for the gain of the amplifiers used, and hence is the output charge of the  
 155 silicon sensor. We expect peak charge of 28,000 and 31,000 electron-hole pairs in a 325  
 156  $\mu\text{m}$  thick silicon detector for ionizing particles with Lorentz factor  $\gamma = 120$  (protons) and  
 157 16,000 (electrons) [12], which is in a good agreement with the measured values. Having  
 158 established the absolute scale of the response using single particles, in our remaining  
 159 studies we normalize all charge measurements to the 120 GeV proton signal, which we  
 160 refer to in the following as  $Q_{\text{MIP}}$ .

161 We study the response of the silicon sensor to electron beams of various energies  
 162 after 6 radiation lengths ( $X_0$ ) of tungsten absorber. The silicon sensor is expected to  
 163 be sensitive to the number of secondary electrons produced within the electromagnetic  
 164 shower, and therefore its response is expected to scale up with higher incident electron

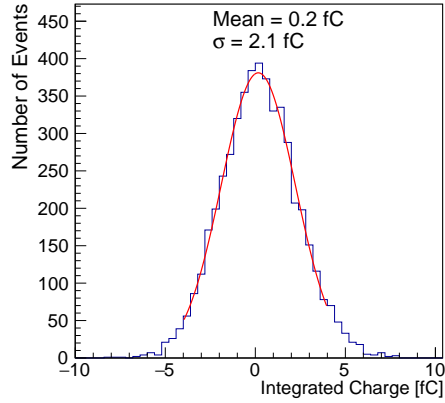


Figure 6: The distribution of charge integrated in the silicon sensor is shown for data events with no beam and random trigger.

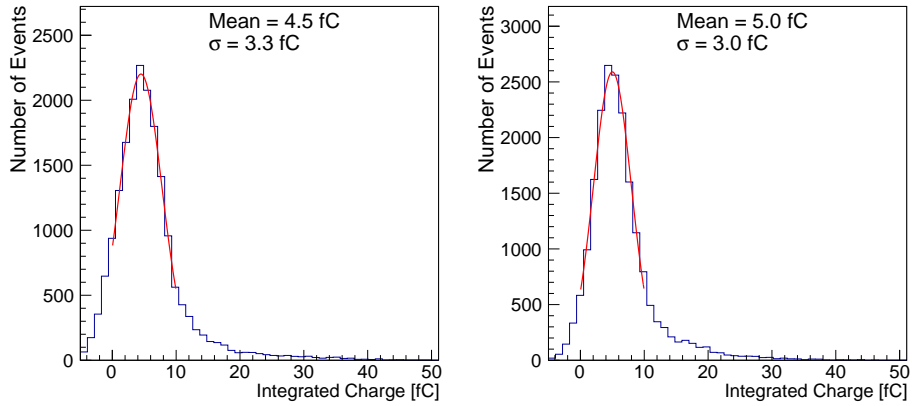


Figure 7: The distribution of charge integrated in the silicon sensor is shown for a beam of 120 GeV protons (left) and 8 GeV electrons (right) without any absorber upstream of the silicon sensor. These conditions mimic the response of the silicon sensor to a minimum-ionizing particle. All triggered events were used in these distributions.

165 energy. In Figure 8, we show an example of the integrated charge distribution measured  
 166 in the silicon sensor after 6 radiation lengths of tungsten, for runs with 32 GeV electrons.  
 167 We show the mean and RMS of these distributions as a function of incident electron beam  
 168 energy in Figure 8. The uncertainties plotted show the RMS of the charge distribution.  
 169 Since the electron beam profile and purity varies at different beam energies, we collected  
 170 between 10 and 50 thousand events for each beam energy, in order to ensure sufficiently  
 171 large data samples. We observe a fairly linear dependence between the measured charge  
 172 and the incident beam energy, for beam energies between 4 GeV and 32 GeV.

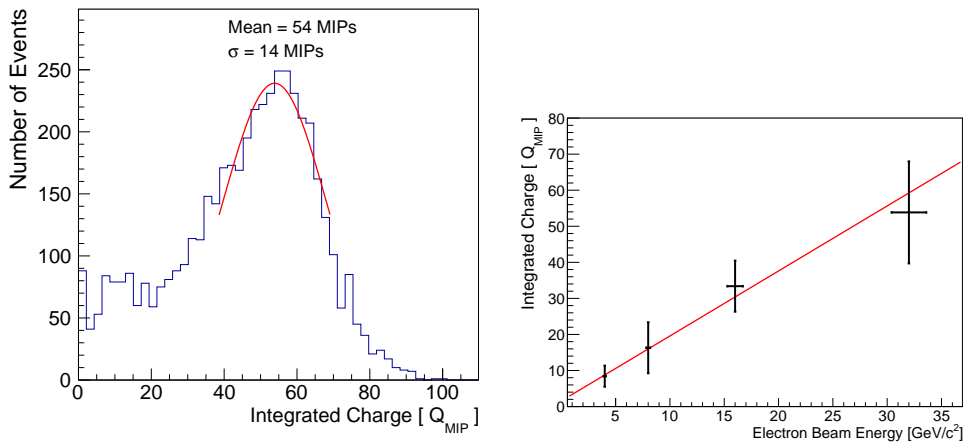


Figure 8: Left: An example of the distribution of integrated charge in the silicon sensor for 32 GeV electrons and 6  $X_0$  absorber shown in units of  $Q_{\text{MIP}}$ . Right: The integrated charge in the silicon sensor expressed in units of  $Q_{\text{MIP}}$  is shown for the same 6  $X_0$  absorber as a function of the electron beam energy. The uncertainty bands show the RMS of the measured charge distribution. The red line is the best fit to a linear function..

173 We also measure the time resolution between the silicon sensor and the Photek MCP-  
 174 PMT, by measuring the standard deviation of the gaussian fit to the distribution of  
 175  $\Delta t = t_0 - t_1$ . We observe a systematic dependence of  $\Delta t$  on the total charge measured  
 176 in the silicon detector, as shown on the left panel in Figure 9. This dependence on the  
 177 integrated charge of the amplified signal was reproduced when we connected the output  
 178 of the pulse generator to the same amplifiers as used in the measurements. We perform  
 179 a correction to  $\Delta t$  for each event using the measured charge in the silicon sensor. This  
 180 procedure is referred to in the following as *time correction*. The correction is obtained  
 181 from a second degree polynomial fit to the distribution of the  $\Delta t$  versus total charge  
 182 collected in the silicon sensor, as shown in Figure 9. We verify that the time correction  
 183 flattens the dependence of the time measurement on the integrated charge, as shown on  
 184 the right panel of Figure 9, and improves the time resolution measurement by 30 – 35%.  
 185 All time resolution measurements in the rest of this study are performed after such a time  
 186 correction. An example of a corrected  $\Delta t$  distribution for 32 GeV electrons after 6  $X_0$  is  
 187 shown on the left of Figure 10. Other than the electron identification requirements, no  
 188 additional selection requirements on the amplitude of the signal in the silicon sensor were  
 189 made. The dependence of the measured time resolution on the beam energy is shown

190 on the right of Figure 10. We observe an improvement in the time resolution as beam  
 191 energy increases, and achieve a time resolution of 23 ps for the 32 GeV electron beam.

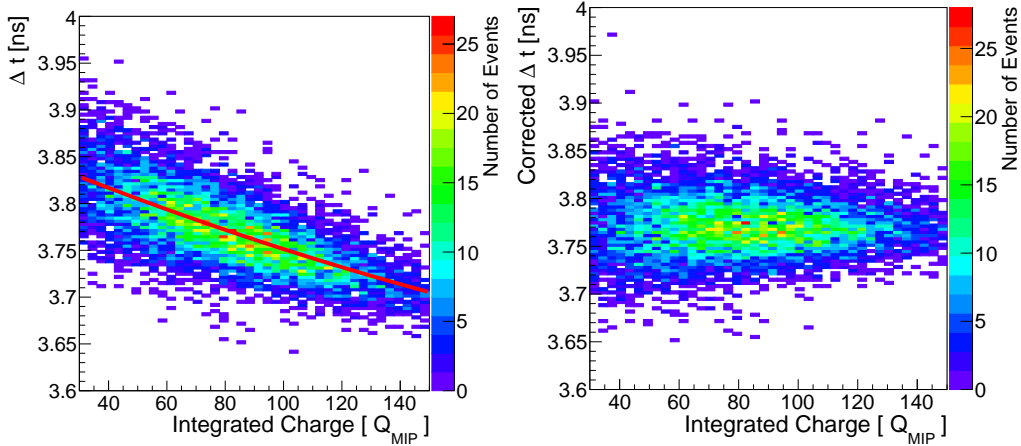


Figure 9: The dependence of  $\Delta t$  on the integrated charge in the silicon sensor is shown on the left. The red curve represents the fit to the profile plot of the two dimensional distribution, and is used to correct  $\Delta t$  for this effect. On the right, we show the corresponding two dimensional distribution after performing the correction. A 16 GeV electron beam is used, and the silicon sensor is placed after 6  $X_0$  of tungsten absorber.

192 Furthermore, we study the response and time resolution of the silicon sensor along  
 193 the longitudinal direction of the shower development. We measure the integrated charge  
 194 and the time resolution as a function of the absorber thickness and present the results  
 195 in Figure 11, for electron beam energy of 8 GeV. A typical longitudinal shower pro-  
 196 file is observed, consistent with previous studies performed using a secondary emission  
 197 calorimeter prototype based on MCP's [3], as well as independent studies of silicon-based  
 198 calorimeter prototypes [13]. The RMS of the integrated charge distribution at each ab-  
 199 sorber thickness is relatively large, due to the small transverse size of the active element  
 200 used in the experiment. We also observe that the time resolution improves as the shower  
 201 develops towards its maximum in the longitudinal direction.

202 Finally, we studied the dependence of the time resolution as a function of the bias  
 203 voltage applied to deplete the silicon sensor. The measurements are shown in Figure 12  
 204 for 16 GeV electrons after 6  $X_0$  of tungsten absorber. We find that the time resolution  
 205 improves as the bias voltage is increased, which is expected on the basis of increased  
 206 velocity of electrons and holes in silicon at larger bias voltage.

## 207 5. Discussion

208 From Figures 6 and 7, we observe that the noise of the prototype system is sufficiently  
 209 low to extract signals from MIPs. Comparing the RMS of the noise distribution with  
 210 the mean of the MIP signal, we find a signal-to-noise ratio around 2 to 2.5. A rough  
 211 estimate from Figure 7 demonstrates that the efficiency to detect 120 GeV protons and

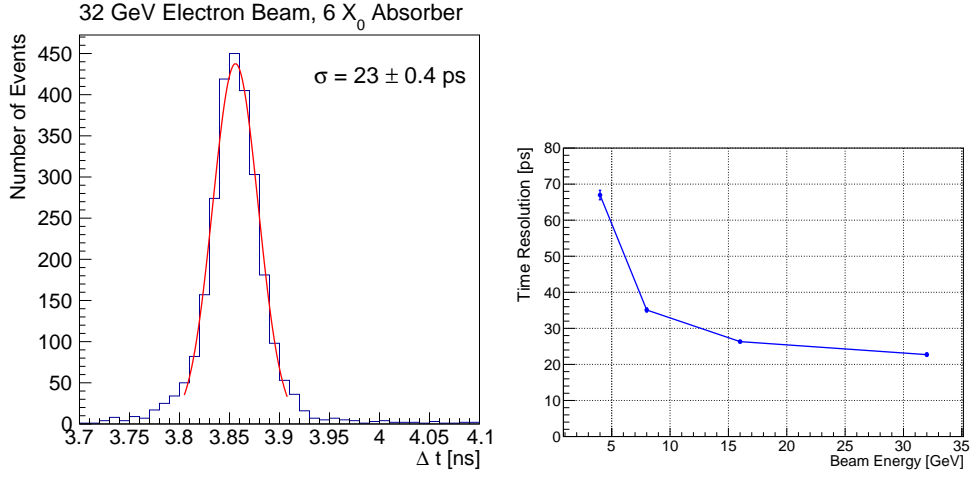


Figure 10: Left: The distribution of  $\Delta t$  between the silicon sensor and the Photek MCP-PMT. A 32 GeV electron beam is used, and the silicon sensor is placed after 6  $X_0$  of tungsten absorber. Right: The measured time resolution between the silicon sensor and the Photek MCP-PMT reference is shown as a function of the electron beam energy. The silicon sensor is placed after 6  $X_0$  of tungsten absorber.

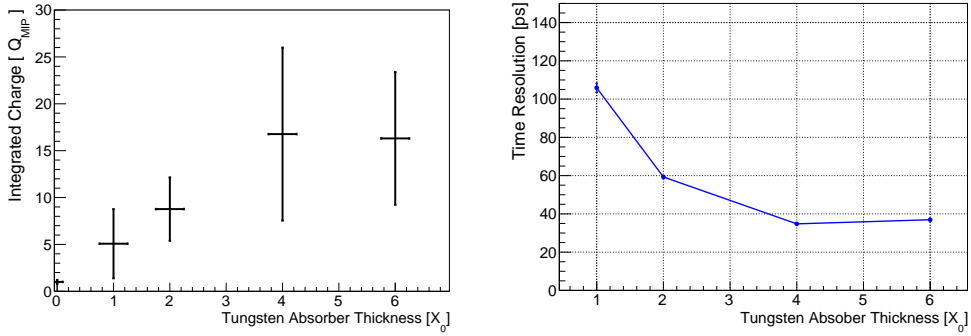


Figure 11: On the left, the integrated charge in the silicon sensor expressed in units of  $Q_{MIP}$  is shown as a function of the absorber (W) thickness measured in units of radiation lengths ( $X_0$ ). The electron beam energy was 8 GeV. The uncertainty bands show the RMS of the measured charge distribution. On the right, the time resolution between the silicon sensor and the Photek MCP-PMT reference is shown as a function of the absorber thickness.

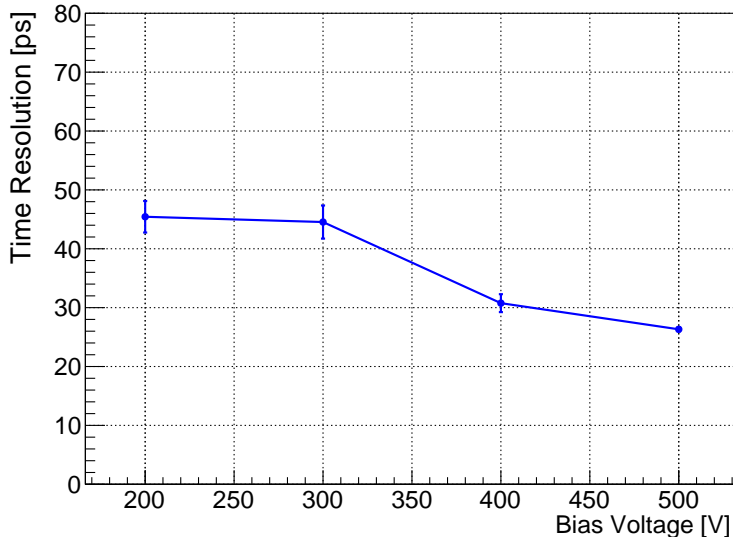


Figure 12: The time resolution between the silicon sensor and the Photech MCP-PMT reference is shown as a function of bias voltage applied on the silicon sensor. The electron beam energy was 16 GeV, and the silicon sensor is placed after 6  $X_0$  of tungsten absorber.

212 8 GeV electrons with no absorber present is larger than 80%. Based on the measurements  
 213 for MIPs, we derive signal distributions for electromagnetic showers normalized to MIP  
 214 response, and observe a relatively linear response to the electron beam energy in the  
 215 range from 4 GeV to 32 GeV after 6  $X_0$  of tungsten absorber, as shown in Figure 10.  
 216 We also measure a longitudinal shower profile in Figure 11 that is consistent with similar  
 217 past measurements.

218 Our results show that the time stamp associated with electromagnetic showers induced  
 219 by electrons with energy between 20 GeV and 30 GeV can be measured with a  
 220 precision better than 25 ps. Results of the measurements reported in Ref. [9] showed  
 221 that a time resolution below 50 ps could be achieved for signals larger than 10 equivalent  
 222 MIPs. We find that the time response of the electronics needs to be well calibrated  
 223 in order to achieve this result. Subtracting 13 ps for the resolution of the reference  
 224 Photech MCP-PMT detector measured with showers [3] yields a precision close to 20 ps.  
 225 Moreover, we observe an improvement of the time resolution with the energy of the electron,  
 226 and more generally with an increase in the signal amplitude. These measurements  
 227 demonstrate that a calorimeter based on silicon sensors as the active medium can achieve  
 228 intrinsic time resolution at the 20 ps level, as long as noise is kept under control. Time  
 229 jitter arising from intrinsic properties of the silicon sensor is demonstrated to be well  
 230 below the 20 ps level.

## 231 6. Conclusion

232 The best time resolution of 23 ps for a silicon sensor was achieved with a 32 GeV beam  
233 and with the silicon sensor placed after 6 radiation lengths of tungsten absorber. Based  
234 on our calibration data for the response of the silicon sensor to MIPs, this measurement  
235 corresponds roughly to an average of 54 secondary particles registered from the electro-  
236 magnetic shower. We observe a roughly linearly increasing response as the energy of the  
237 electron beam is increased, and we observe a longitudinal shower profile consistent with  
238 similar past measurements. This result yields further encouragement to use silicon for  
239 active layers in calorimeters, as is planned for example for the CMS Phase 2 upgrade [7],  
240 and explicitly demonstrates the opportunity to use silicon for timing measurements in  
241 future calorimeters. To continue, we plan to extend our studies to more realistic proto-  
242 types covering larger transverse and longitudinal regions of the electromagnetic shower  
243 and using multiple channels.

## 244 7. Acknowledgements

245 Operated by Fermi Research Alliance, LLC under Contract No. DE-AC02-07CH11359  
246 with the United States Department of Energy. Supported by funding from California  
247 Institute of Technology High Energy Physics under Contract DE-SC0011925 with the  
248 United States Department of Energy. We thank the FTBF personnel for very good  
249 beam conditions during our test beam time. We also appreciate the technical support of  
250 the Fermilab SiDet department for the production of high quality silicon samples.

## 251 References

- 252 [1] D. Anderson, A. Apresyan, A. Bornheim, J. Duarte, C. Pena, A. Ronzhin, M. Spiropulu, J. Trevor,  
253 and S. Xie, “On Timing Properties of LYSO-Based Calorimeters,” *Nucl. Instrum. Meth. A*, vol. 794,  
254 pp. 7–14, 2015.
- 255 [2] A. Ronzhin, S. Los, E. Ramberg, M. Spiropulu, A. Apresyan, S. Xie, H. Kim, and A. Zatserklyaniy,  
256 “Development of a new fast shower maximum detector based on microchannel plates photomulti-  
257 pliers (MCP-PMT) as an active element,” *Nucl. Instrum. Meth. A*, vol. 759, pp. 65 – 73, 2014.
- 258 [3] A. Ronzhin, S. Los, E. Ramberg, A. Apresyan, S. Xie, M. Spiropulu, and H. Kim, “Study of the  
259 timing performance of micro-channel plate photomultiplier for use as an active layer in a shower  
260 maximum detector,” *Nucl. Instrum. Meth. A*, vol. 795, pp. 288 – 292, 2015.
- 261 [4] A. Ronzhin, S. Los, E. Ramberg, A. Apresyan, S. Xie, M. Spiropulu, and H. Kim, “Direct tests  
262 of micro channel plates as the active element of a new shower maximum detector,” *Nucl. Instrum.*  
263 *Meth. A*, vol. 795, pp. 52 – 57, 2015.
- 264 [5] L. Brianza, F. Cavallari, D. Del Re, S. Gelli, A. Ghezzi, C. Gotti, P. Govoni, C. Jorda Lopez, A.  
265 Martelli, B. Marzocchi, P. Meridiani, G. Organtini, R. Paramatti, L. Pernie, S. Pigazzini, S. Ra-  
266 hatlou, C. Rovelli, F. Santanastasio, T. Tabarelli de Fatis, N. Trevisani, “Response of microchannel  
267 plates to single particles and to electromagnetic showers,” *Nucl. Instrum. Meth. A*, vol. 797, pp. 216  
268 – 221, 2015.
- 269 [6] C. Adloff, J. Blaha, J. J. Blaising, C. Drancourt, A. Espargiliere, R. Galione, N. Geffroy, Y. Kary-  
270 otakis, J. Prast, and G. Vouters, “Tests of a particle flow algorithm with CALICE test beam data,”  
271 *JINST*, vol. 6, p. P07005, 2011.
- 272 [7] J. Butler, D. Contardo, M. Klute, J. Mans, and L. Silvestris, “Technical Proposal for the Phase-II  
273 Upgrade of the CMS Detector,” Tech. Rep. CERN-LHCC-2015-010. LHCC-P-008, CERN, Geneva,  
274 Jun 2015.
- 275 [8] [https://www.hamamatsu.com/resources/pdf/ssd/e10\\_handbook\\_for\\_high\\_energy.pdf](https://www.hamamatsu.com/resources/pdf/ssd/e10_handbook_for_high_energy.pdf).
- 276 [9] N. Akchurin *et al.*, “On the timing performance of thin planar silicon sensors.” In preparation, for  
277 submission to the Nucl. Instrum. Meth. A.

- 278 [10] <http://www.caen.it/csite/CaenProd.jsp?parent=11&idmod=661>.
- 279 [11] H. Kim, C.-T. Chen, N. Eclov, A. Ronzhin, P. Murat, E. Ramberg, S. Los, W. Moses, W.-S. Choong,  
280 and C.-M. Kao, “A new time calibration method for switched-capacitor-array-based waveform sam-  
281 plers,” *Nucl. Instrum. Meth. A*, vol. 767, pp. 67 – 74, 2014.
- 282 [12] K. A. Olive *et al.*, “Review of Particle Physics,” *Chin. Phys.*, vol. C38, p. 090001, 2014.
- 283 [13] S. Muhuri, S. Mukhopadhyay, V. B. Chandratre, M. Sukhwani, S. Jena, S. A. Khan, T. K. Nayak,  
284 J. Saini, and R. N. Singaraju, “Test and characterization of a prototype silicon-tungsten electro-  
285 magnetic calorimeter,” *Nucl. Instrum. Meth. A*, vol. 764, pp. 24 – 29, 2014.